communications earth & environment

Article

https://doi.org/10.1038/s43247-024-01418-3

Coastal ecological disasters triggered by an extreme rainfall event thousands of kilometers inland

Wenjian Li[1], Zhenyan Wang[1,2,3,4] ✉, Quanchao Cui[1,3,5], Xiaole Sun[3,5] & Haijun Huang[1,3]

The world is experiencing an increase in the frequency and intensity of extreme weather events, yet the influences of remote inland extreme weather events on the coastal ecosystem thousands of kilometers away remain poorly understood. Here we tracked the chain ecological effects of an extreme rainfall event in North China from terrestrial rivers to coastal aquaculture area of the eastern Shandong Peninsula. Our data suggest the autumn flood resulted from extreme rainfall event leads to abnormally low turbidity in the North Shandong Coastal Currents and coastal red tide blooms by introducing anomalous freshwater with an exceptionally high nitrogen-to-phosphorus ratio into the Bohai Sea. Lower salinity, stronger light conditions caused by limpid coastal currents, and phosphorus limitation resulting from red tide blooms account for huge kelp loss offshore of the eastern Shandong Peninsula. This study underscores the importance of considering multidisciplinary observation for risk management of unexpected extreme weather events.

Coastal zones, serving as vital interfaces between land and the ocean, have become focal points for dynamic socio-economic development and have exhibited increased sensitivity to the effects of climate change[1,2]. Extreme weather events, like storms, tsunamis, and coastal flooding, can rapidly alter the structure and function of coastal ecosystems, resulting in severe ecological damage and substantial economic losses when they arrive[3–5]. However, the influence of extreme weather events in remote inland areas on the ecological environment and aquaculture industry of coastal zones is still rarely reported, and the underlying transference mechanisms remain poorly understood.

Kelps serve as one of the most important aquaculture species and function as foundation species in coastal ecosystems, providing habitat, nursery ground, and food for thousands of organisms[6]. China boasts the world's largest kelp cultivation industry. The aquaculture area and yield of fresh kelp in Rongcheng City on the eastern coast of the Shandong Peninsula both rank first in China[7,8] (Fig. 1). However, in November 2021, Rongcheng City experienced the worst kelp mortality on record, accompanied by severe red tide blooms[9]. Consequently, the kelp (*Saccharina Japonica*) yield in Rongcheng City was almost extinct in 2022, resulting in an estimated direct economic loss of nearly 200 million Chinese Yuan[10]. The 2021–2022 kelp mortality event has dealt a devastating blow to local aquaculture industry. Investigations conducted in situ post-event have determined that this ecological disaster was attributed to abnormally high water transparency and a severe depletion of phosphate in seawater[10]. Nevertheless, the reasons for the increase in water transparency and nutrient deficiency remain unclear. Event attribution and underlying mechanism elucidation of this kelp mortality event on larger spatiotemporal scales remain to be further studied.

Previous studies revealed that, wind-driven waves caused bottom sediment resuspension and the release of nutrients carried by sediment particles during the winter half-year, which promoted the growth of plankton along coast of the Shandong Peninsula[11,12]. The weakening of the wind speed was considered a primary factor in the reduction of suspended sediment concentration (SSC) and thus higher water transparency in the coastal area of Bohai and North Yellow Sea[12,13], and the proportion of plankton in sediment particles was negligible[11]. However, no abnormalities were observed in the wind field during the autumn of 2021. The underlying cause of this anomalous environmental fluctuation remains elusive. It is worth noting that two months before the kelp mortality event, continuous extreme rainfall was strikingly recorded over North China in the autumn of 2021, causing an unexpected autumn flood in the Yellow River. Does the autumn extreme rainfall event in North China have a causal relationship with the kelp mortality event so far away, and what are the intrinsic

[1]CAS Key Laboratory of Marine Geology and Environment, Institute of Oceanology, Chinese Academy of Sciences, Qingdao 266071, China. [2]Laboratory for Marine Mineral Resources, Qingdao Marine Science and Technology Center, Qingdao 266237, China. [3]University of Chinese Academy of Sciences, Beijing 100049, China. [4]Shandong University of Science and Technology, Qingdao 266590, China. [5]Center of Deep Sea Research, Institute of Oceanology, Chinese Academy of Sciences, Qingdao 266071, China. ✉e-mail: zywang@qdio.ac.cn

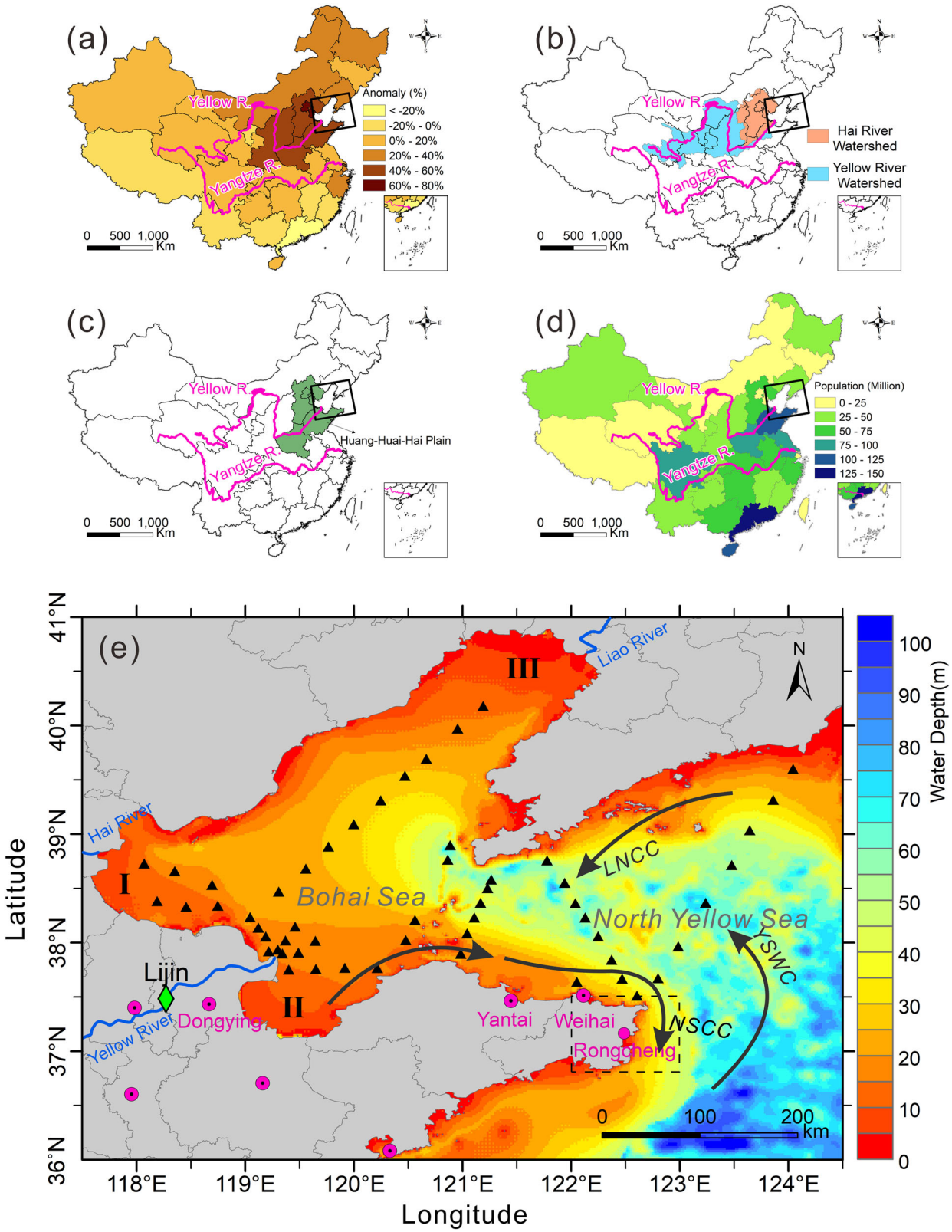

Fig. 1 | Geographic and hydroclimate context of the study area. a Horizontal distribution of the rainfall anomalies of each province in China in 2021. The magenta lines indicate the large rivers. The black solid box indicates the study area in **e**. **b** The location of Yellow River watershed and Hai River watershed. **c** The location of Huang-Huai-Hai plain. **d** Horizontal distribution of the population (million) of each province in China. **e** Bathymetric map of the Bohai Sea and North Yellow Sea with the locations of the survey stations (black solid triangles). The magenta circles indicate the cities of Shandong Province. The green rhombus indicates the gauge station of Lijin. The blue solid line indicates the Yellow River, Hai River, and Liao River. The dashed box indicates the Rongcheng offshore area where the MODIS imageries are averaged in Fig. 8. The arrows indicate the ocean current of North Shandong Coastal Current (NSCC), Yellow Sea Warm Current (YSWC) and Liaonan Coastal Current (LNCC). The Roman numerals indicate the location of I Bohai Bay, II Laizhou Bay, and III Liaodong Bay.

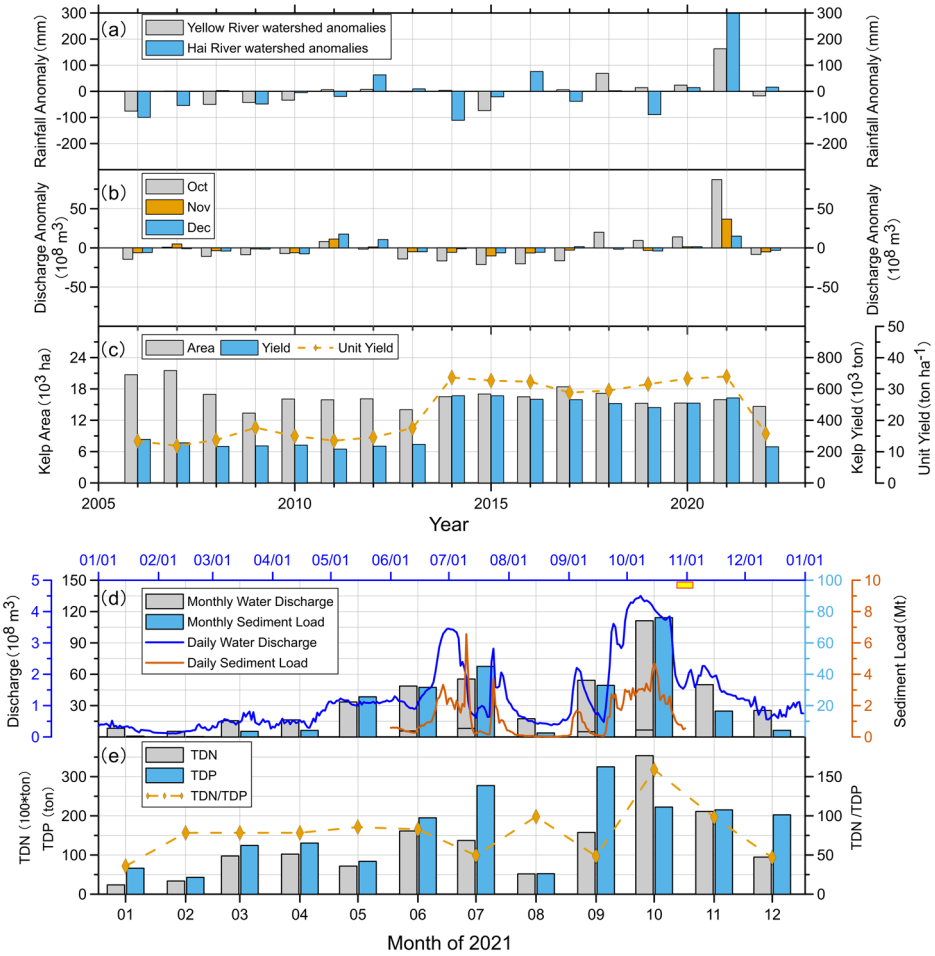

Fig. 2 | Time series of rainfall, river discharge, and sediment load from the Yellow River, and kelp area and yield of Shandong province. a The annual rainfall anomalies in the Yellow River (gray columns) and Hai River (blue columns) watershed spanning from 2006 to 2022. **b** The autumn water discharge anomalies (~10^8 m^3) of Yellow River in October (gray columns), November (orange columns), and December (blue column) recorded at gauging stations of Lijin spanning from 2006 to 2022. **c** Annual kelp area, yield, and unit yield of Shandong province spanning from 2006 to 2022. **d** The monthly water discharge (~10^8 m^3; gray columns) and sediment loads (Mt; blue columns) of Yellow River recorded at gauging stations of Lijin in 2021. The blue and orange solid lines indicate the daily water flux and sediment load, respectively. The yellow box indicates the cruise survey time (27 October 2021–04 November 2021). **e** The monthly flux of total dissolved nitrogen (TDN; gray columns), total dissolved phosphorus (TDP; blue columns), and TDN/TDP ratio (orange lines) of Yellow River recorded at the gauging station of Lijin in 2021.

mechanisms involved? Here, we aim to combine field observations (Supplementary Fig. S1) with contemporaneous satellite remote sensing data to unveil the relationship and underlying transference mechanism between remote inland extreme rainfall events and coastal kelp mortality events thousands of kilometers away. This provides a unique opportunity to examine the teleconnection of global climate change on regional marine ecosystems through a comprehensive assessment of physical, chemical, and biological cascading effects.

Results and discussion

Inland extreme rainfall events led to autumn flood of the Yellow River and phosphorus limitation of the Bohai Sea

In summer, the East Asian climate is regulated by a high-pressure system, called Western North Pacific Subtropical High (WNPSH)[14]. The WNPSH transports water vapor subtropical western North Pacific into East Asia through southerly wind, and anchors the rain belt on its northwestern periphery where a convergence of moist southerly winds and cold air masses occurs[15]. Anomalous intrusion or deficiency of the WNPSH can lead to extreme weather events such as floods, droughts, and heat waves in East Asia[16]. In 2021, North China experienced its wettest autumn since 1961, accompanied by record-breaking rainfall that nearly doubled the average rainfall in the same period of previous years (Fig. 2a, b). This extreme wet condition of North China in autumn 2021 was also attributed to the westward inland intrusion of the WNPSH, triggered by higher sea surface temperature anomalies (SSTA) in the Indo-Pacific warm pool[17]. The annual rainfall anomalies reached the highest historical values of 162.9 mm (equivalent to 1314.5×10^8 m^3) and 300.3 mm (equivalent to 1105.4×10^8 m^3) in the Yellow River and Hai River watersheds, respectively (Fig. 2a, b). Consequently, the heavy floods that occurred in both the Yellow River and Hai River basins broke historical records despite the Yellow River having a much higher discharge compared to the Hai River (Fig. 2d and Supplementary Fig. S2).

In 2021, the time series of Yellow River discharge exhibited an unusual bimodal distribution, with peaks observed in the summer (June and July) and the highest peak recorded in autumn (October and November) (Fig. 2d). The sediment loads exhibited a double-peak distribution resembling discharge, albeit with a more constricted peak width. Sediment load increased rapidly with the onset of flooding, peaking in mid-October. However, it subsequently dropped rapidly to less than 1 Mt at the end of October, while the discharge gradually decreased until December, returning to pre-flood levels. Therefore, the river input was characterized by high river discharge but low sediment loads from late October to early November during the cruise survey period (Fig. 2d), i.e., the water-sediment separation. This pattern was confirmed by the lower turbidity around the Yellow River estuary, i.e., the hyposaline water dominated Laizhou Bay and Bohai Bay, while the turbidity was even lower than that in southern Bohai Strait (Fig. 3b, d).

The impact of the 2021 autumn flood extended to the southwestern Bohai Sea, lowering salinity to levels below 30, resulting in a pronounced salinity front outside Bohai Bay and Laizhou Bay (Fig. 3b). High chl-a concentrations were observed along this salinity front in surface layer, indicating notable phytoplankton blooms (Fig. 3c). Bohai Bay and Laizhou Bay exhibited low salinity and high nutrient concentration of DIN and DSi, coupled with an anomalous high DIN/DIP ratio (Fig. 3e–h). Submarine Groundwater Discharge was recognized as a potentially critical factor influencing the excessive nutrients present in the Bohai Sea[18,19]. Nevertheless, an examination of the vertical distribution of nutrients revealed that DIN and DSi originated from surface layers rather than the bottom layer

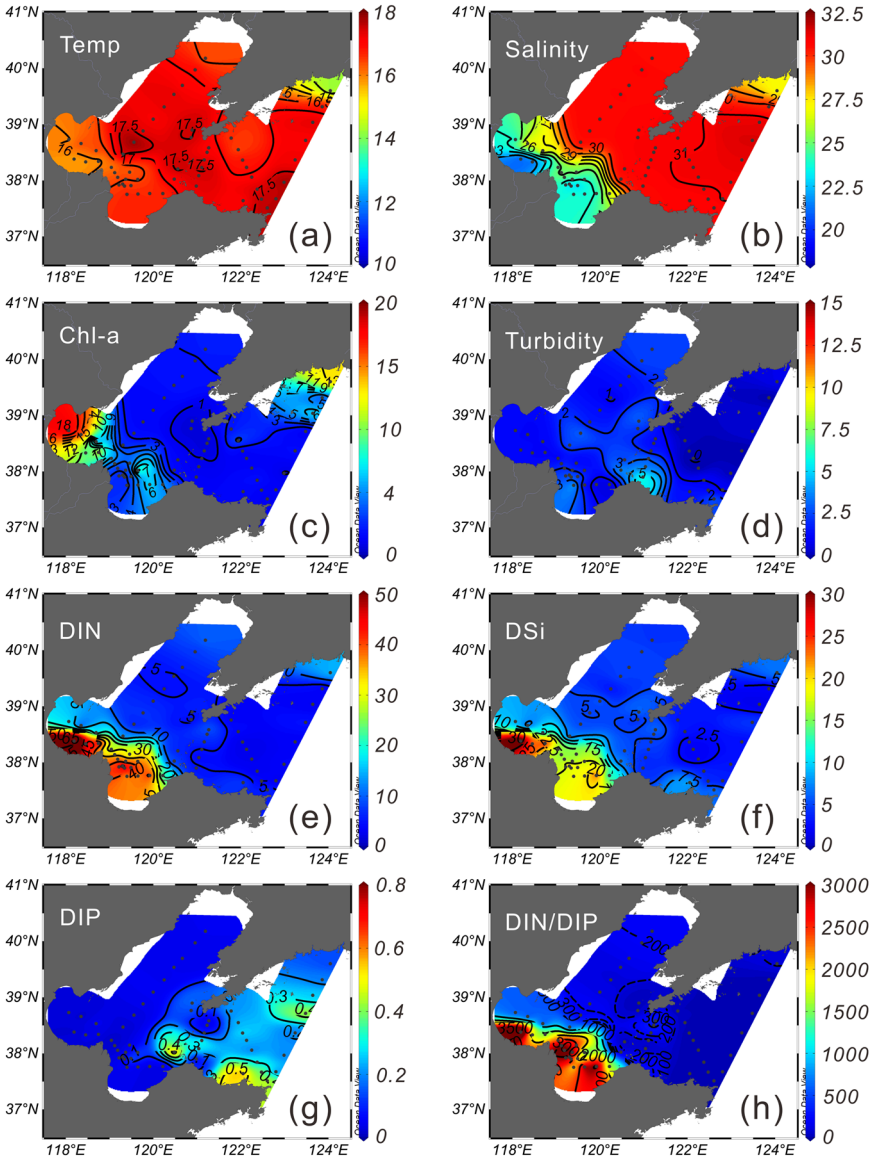

Fig. 3 | Horizontal distribution of hydrological parameters in surface layer over Bohai and North Yellow Sea in autumn 2021 (October 27–November 04). **a** Water temperature (°C); **b** Water salinity; **c** Chl-a concentration (mg m^{-3}); **d** Turbidity (NTU); **e** DIN (μmol L^{-1}); **f** DSi (μmol/L); **g** DIP (μmol L^{-1}), and **h** DIN/DIP.

(Supplementary Fig. S3e1, f1), suggesting a dominant influence from river discharge[20]. As the Yellow River flows through the Huang-Huai-Hai agricultural area, one of China's largest agricultural production bases, the increase in population and anthropogenic fertilizer application has contributed to higher nutrient transport via rivers during the last decades[21] (Fig.1c, d). It was reported that fertilizer loss in DIN (44–48%), sewage effluents in DIP (85–88%), and natural runoff in DSi (35–65%) were the largest contributors to total nutrient flux in the Yellow River discharge respectively[22,23]. During the autumn flood of 2021, there was a considerable influx of nutrients from the Yellow River into the Bohai Sea (Fig. 2e). Notably, the peak nutrient fluxes during this autumn season surpassed those observed during the summer flood season, with the highest TDN/TDP ratio recorded. The good negative correlation between nutrient concentrations of DIN, DSi, and salinity further confirmed the contribution of river discharge[24] (Supplementary Fig. S4a, b). However, the DIP was mainly derived from sediment resuspension since it positively correlated with turbidity rather than salinity (Supplementary Fig. S4c, d). As phytoplankton growth consumed large amounts of DIP, extremely high DIN:DIP ratio of over 3000 occurred in the Bohai Sea (Fig. 3h), which considerably exceeded that reported ratio in previous studies[24,25] (Fig. 4a). The strong linear correlation between DIN:DIP ratio and DSi:DIP ratio (slope = 1.13, $r = 0.99$, $p < 0.001$) indicated that DIN and DSi had the same source of river input related to the autumn flood as well[24,26] (Fig. 4a). The Redfield ratio[27] analysis confirmed that the Bohai Sea experienced severe phosphorus limitation in surface layer, while the North Yellow Sea experienced silicon limitation (Fig. 4). Nitrogen limitation was observed only at several stations along the northern coast of the Shandong Peninsula. In summary, extreme rainfall-induced autumn floods carried large amounts of nutrients into the Bohai Sea, resulting in eutrophication and subsequent phytoplankton blooms there.

Anomalous limpid coastal current caused by autumn flood of the Yellow River

The North Shandong Coastal Current (NSCC) has traditionally been known as the primary carrier of sediments from the Yellow River, transporting them from the Bohai Sea to the Yellow Sea along the coast of the Shandong Peninsula during winter season[28] (Fig. 1e). Thus it was typically characterized by low-salinity, cold and highly turbid water belt along the coast of Shandong Peninsula[29,30]. Then, temperature fronts usually formed between the cold NSCC and the warm Yellow Sea Warm Current (YSWC) during the winter season[31].

Climatically, pronounced sea surface temperature gradients (SSTGs) emerged in November and intensified by December (Supplementary Fig. S5a–c). However, in November 2021, the notable SSTGs exceeded

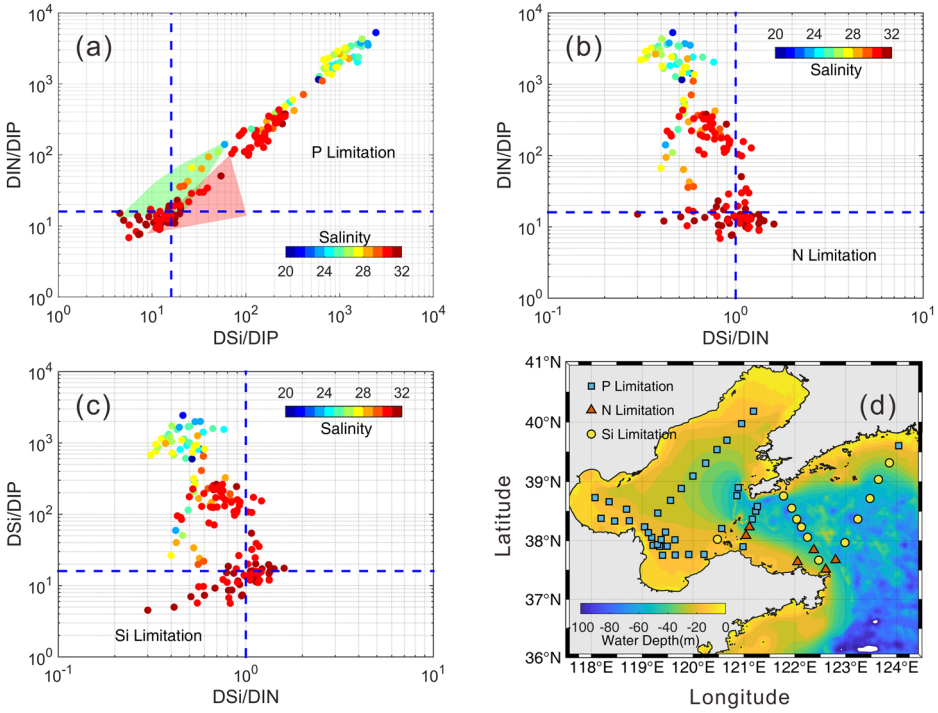

Fig. 4 | Nutrient status in the surface layer of the Bohai and North Yellow Sea. a–c Scatter of DIN, DSi, and DIP based on the cruise survey data. The blue dashed lines indicate the criteria to identify the nutrient conditions according to the Redfield ratio (C:N:Si:P = 106:16:16:1). The red and green patches in **a** indicate the measured molar ratios of DIN:DIP in Bohai Sea cited from ref. 24,25. The classification of stations based on the nutrient conditions (**d**). The blue squares, red triangles, and yellow circles indicate the stations with phosphorus limitation, nitrogen limitation, and silicon limitation, respectively.

0.05 °C km^{-1} along the northern coast of the Shandong Peninsula (Supplementary Fig. S5d–f). The SSTG anomalies surpassing 0.02 °C km^{-1} when compared to the climatological mean state along the northern coast of the Shandong Peninsula (Fig. 5a, b), which indicated an early intrusion of cold NSCC along this region. Intriguingly, the northern coast of the Shandong Peninsula displayed serious negative SSC anomalies during November 2021 (Fig. 5c). This was a notable deviation from the high turbidity typically associated with NSCC. The spatial distribution of SSC anomalies suggested their origin in the Yellow River Estuary area. As discussed before, the autumn floods of 2021 resulted in the water-sediment separation in the estuary area (Fig. 2d). Freshwater with low SSC was spread from the Bohai Sea to the Yellow Sea driven by NSCC in November. Consequently, the severe autumn flood of 2021, coupled with water-sediment separation, led to anomalous limpid NSCC.

Shipboard acoustic Doppler current profiler (ADCP) observation confirmed the early intrusion of NSCC along the northern coast of Shandong Peninsula on 02 November 2021 (Fig. 6). It revealed a two-layer flow structure, with the velocity vector rotating in the opposite direction to the west of 122.5°E in November (Fig. 6a). The buoyant surface NSCC flowed eastward at a velocity of over 1000 mm s^{-1}, while the heavier bottom water below 9 m flowed westward at a velocity of <300 mm s^{-1}. The water columns exhibited a two-layer hydrological structure at station W1 accordingly, with pycnocline occurred between fresher surface water and saltier bottom water (Fig. 6c). The pycnocline acted as a barrier, inhibiting the upward diffusion of resuspended sediments from the bottom nepheloid layers as indicated by the vertical distribution of backscattering strength of suspended particles (S_v) (Fig. 6b). As the current progressed from station W1 to CD1, the influence of the advection diminished, and the resuspended sediments gradually increased (Fig. 6b). The water column also switched from stratified status to vertical mixing, which was manifested by the uniform vertical distribution of low buoyant frequency ($N^2 < 0$) (Fig. 6c).

Satellite imagery provided insights into the temporal evolution of NSCC from a broader spatiotemporal perspective. In October 2021, the SSTG had not yet manifested, whereas the turbid water belt was observed along the coast of the Shandong Peninsula (Fig. 7a, b, i, j). However, as the autumn flood of 2021 occurred and the water-sediment separation took place, an anomalous limpid NSCC was formed by November 12 (Fig. 7c, d). At the same time, the low-turbidity water belt appeared along the northern coast of Shandong Peninsula (Fig. 7k, l). The Landsat-8 OLI true color images also revealed that the sediment-laden water has been replaced by clear water along the north coast of Shandong Peninsula from October 29 to November 14 (Supplementary Fig. S6). From November 14–27, NSCC bypassed Cape Chengshan and reached the coastal area of Rongcheng city (Fig. 7d–h). Concurrently, the low-turbidity water belt expanded alongside the expansion of the NSCC (Fig. 7l–p). The buoy observation of low salinity also confirmed the intrusion of NSCC in November 2021 compared with previous years (Supplementary Fig. S7c).

The red tide bloomed in the salinity frontal zone and migrated with coastal currents

During the autumn of 2021, the Bohai Sea exhibited severe phosphorus limitation (Figs. 3 and 4). The distribution of high chl-a concentration, indicating phytoplankton blooms, was observed along the salinity front where DIN and DSi-rich coastal water contacted with DIP-rich waters, rather than in the estuary area (Fig. 3). The physical processes of cross-front convergence and strong along-front advection created more favorable nutrient conditions within the frontal zones that would enhance primary productivity[32]. This pattern of bloom patches was also captured by MODIS (Moderate-resolution Imaging Spectroradiometer) satellite images (Fig. 7r). Furthermore, the NSCC transported DIN- and DSi-rich waters to the Yellow Sea over time, constantly meeting DIP-rich local water along the coast of the Shandong Peninsula (Supplementary Fig. S3g1–g4). This continuous process of nutrient enrichment in the frontal zone was highly favorable for the occurrence of phytoplankton blooms.

The Bulletin of China Marine Disaster in 2021 reported two large-scale red tide blooms in Bohai and North Yellow Sea during the autumn season[9]. The first red tide bloom occurred from October 27 to November 05 in the coastal area of Dongying City, covering an area of 1052 km^2. The average abundances in Laizhou Bay on October 2021 were 4.2×10^5 cells L^{-1}, while high abundances exceeding 1.0×10^6 cells L^{-1} in the western and southern coastal areas[33]. The dominant algae species during this bloom were the dinoflagellates *Akashiwo sanguinea* and *Gonyaulax polygramma*. The second red tide bloom, dominated by the dinoflagellate *Gonyaulax polygramma* occurred in the coastal area of Yantai and Weihai Cities from November 27 to December 16, covering an area of 921 km^2. The distribution of the red tide bloom patches aligned with the locations of high MODIS chl-

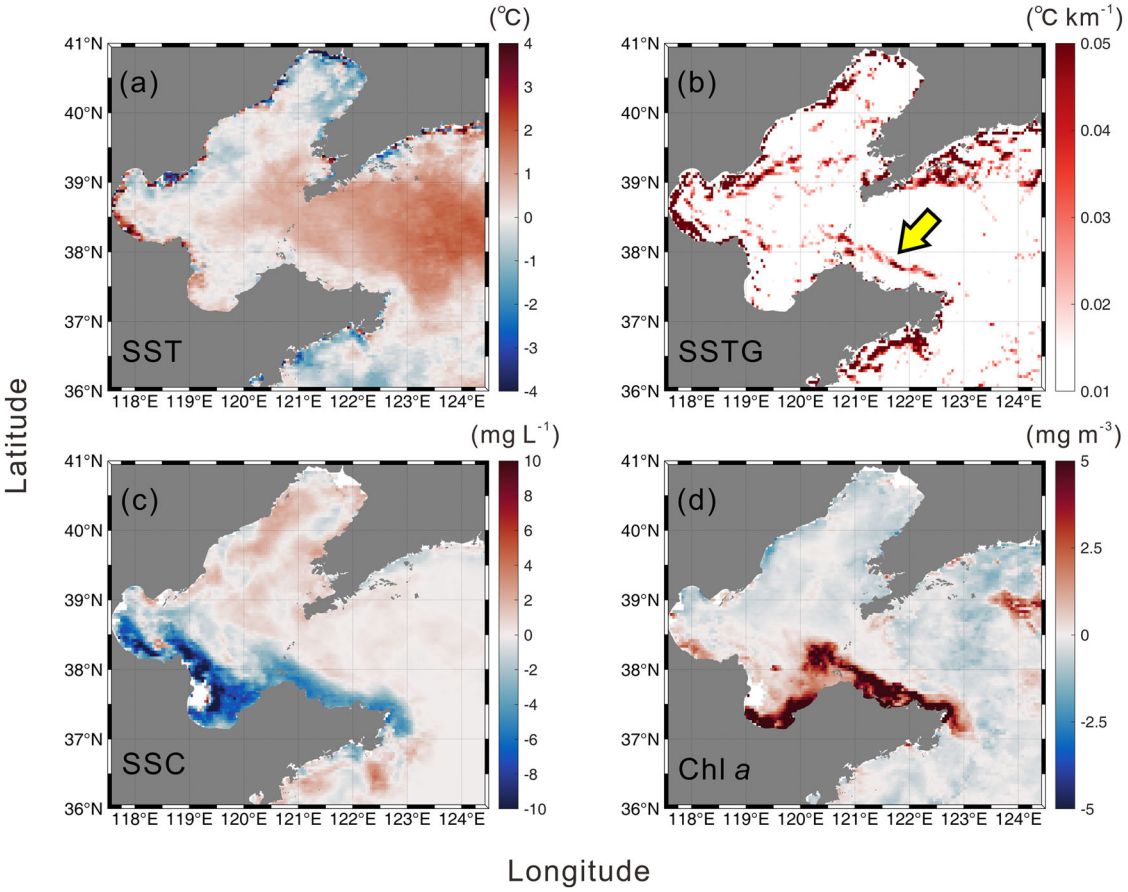

Fig. 5 | Monthly anomalies of MODIS-derived sea surface parameters over the Bohai and North Yellow Sea in November 2021. a SST; **b** SSTG; **c** SSC; and **d** chl-a concentration. The yellow arrow in **b** indicates the front anomalies. The white areas are masked by clouds or bad results from the retrieve algorithm.

a concentration (>10 mg m^{-3}) (Fig. 7q–x), particularly outside of Bohai Bay and Laizhou Bay (Dongying nearshore waters) on October 27 (Fig. 7r). This consistency proved the high chl-a concentration mainly resulted from the red tide blooms in Bohai and North Yellow Sea during autumn of 2021. They expanded along the coast of Shandong Peninsula with the migration of limpid NSCC (Fig. 7). Consequently, the anomalies in the chl-a concentration observed in November 2021 reached levels exceeding 5 mg m^{-3} along the north coast of Shandong Peninsula (Fig. 5d).

As mentioned before, the limpid NSCC dominated the northern coast of the Shandong Peninsula by November 14 (Fig. 7). The nutrient-rich waters transported by the NSCC likely fertilized the red tide blooms in the coastal area of Yantai city on November 14 (Fig. 7t). Over the second half of November, the red tide blooms gradually expanded along the coast of the Shandong Peninsula and bypassed Cape Chengshan to reach the Rongcheng coast (Fig. 7u–x), which were consistent with the movement of the limpid NSCC (Fig. 7e–h). The underlying mechanism was likely the movement of optimal nutrient conditions at the frontal zones created by the interaction of DIN and DSi-rich NSCC and the DIP-rich coastal waters. However, following red tide blooms, nutrient consumption from organic matter decomposition resulted in the establishment of oligotrophic conditions, particularly phosphorus limitation. This poses a conspicuous threat to the survival of local kelp species[10].

Attribution of kelp mortality event to extreme rainfall events

While the kelp farming area in Shandong Province has remained relatively constant over the past decade, both kelp yield and unit yield (yield: area) have more than doubled since 2014 (Fig. 2c). This surge is likely attributed to advancements in farming technology. Unexpectedly, following the extreme rainfall event in the autumn of 2021, kelp yield in Shandong Province experienced a precipitous decline in 2022, reaching levels seen before 2014. Water quality testing conducted immediately after the kelp mortality event in December 2021 found that the contents of agricultural herbicides, pesticides, and heavy metals were all within acceptable aquaculture standards, indicating that there was no presence of lethal chemical agents in the seawater[10].

It was reported that various environmental factors, such as temperature, salinity, nutrient enrichment, and irradiance conditions, could positively affect kelp cultivation[34,35]. However, the combined effects of these factors on kelp growth remained complex and require further research[35]. Kelps were known to be highly tolerant of low temperatures but sensitive to high temperatures due to their adaptation to cold seas[36]. Excessive photosynthetically available radiation (PAR) could inhibit photosynthesis and lead to cellular damage in kelp[37,38]. Nevertheless, the autumn SST and PAR have shown minimal fluctuations over the last 20 years (2002–2021) (Fig. 8b, c and Supplementary Fig. S7b), suggesting they were not the dominant factors causing this mass mortality event of kelp. The lag-correlation analysis also showed that there was no significant correlation between them and kelp unit yield from 2014 to 2021 (Fig. 8h, i). The impact of wind has also been excluded, as no abnormality was observed (Fig. 8a, g and Supplementary Fig. S7a). Unexpectedly, there were close negative relationships between SSC, chl-a concentration and kelp unit yield (Fig. 8j, k). At the interannual scale, high SSC implies a weakening of light conditions, while high chl-a indicates phytoplankton nutrient consumption, both of which are unfavorable for algal photosynthesis and lead to decreased kelp yield. When extreme weather events occurred, the anomalous high concentration of chl-a contributed to a marked decrease in the unit yield of kelp due to severe nutrient consumption. However, the relationship between SSC and unit yield of kelp deviated from the expected development law, causing unpredictable ecological processes.

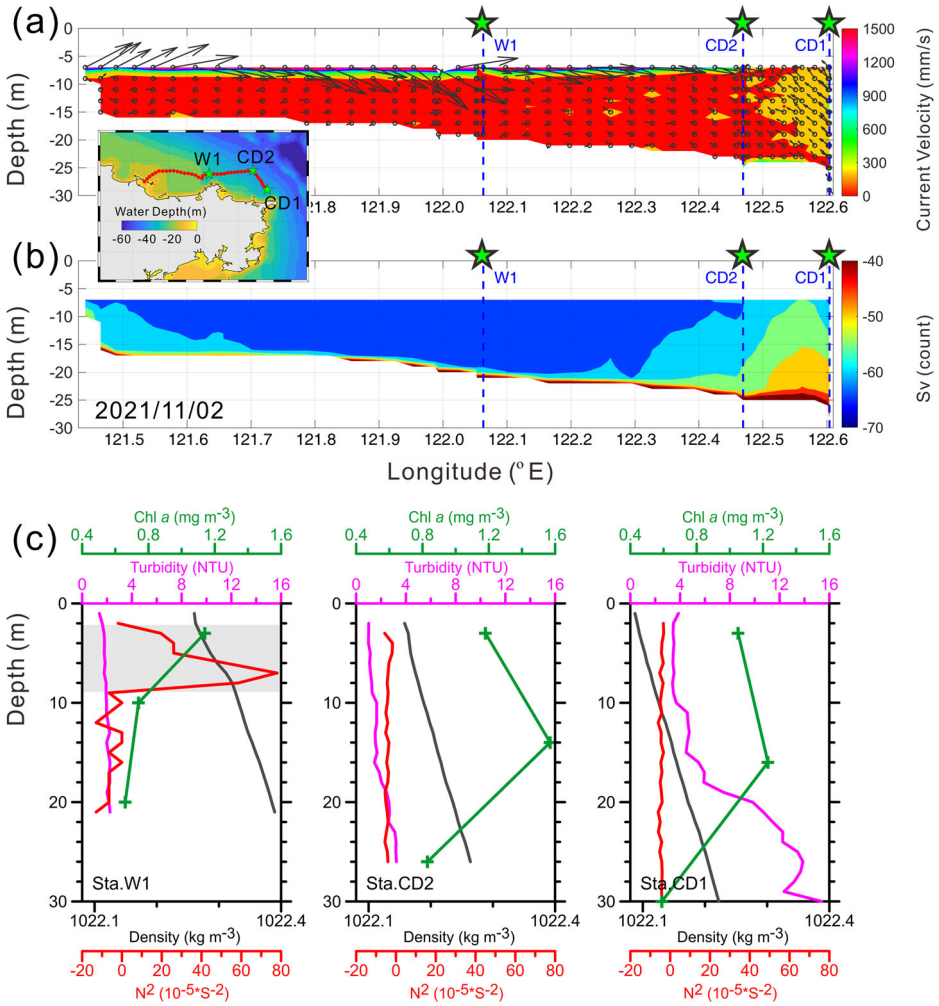

Fig. 6 | Vertical distribution of hydrodynamic conditions from cruise survey in 02 November 2021. a The section of subtidal current velocity (mm s^{-1}) measured by ADCP along the offshore of the north coast of Shandong Peninsula. **b** Same as **a** but for S_v (count). **c** Hydrological profile of water density (gray), buoyant frequency (red), turbidity (magenta), and chl-a concentration (grass green) at station W1, CD2, and CD1 as shown with green stars in **a**, **b**.

The seawater along the coast of Shandong Peninsula in November 2021 exhibited the lowest SSC (4.69 mg L^{-1}) and the highest chl-a concentration (7.03 mg m^3) in the same period in history (Fig. 8d, e). On the one hand, kelp seedlings were typically transferred from land-based hatchery to the offshore facilities in the Rongcheng kelp farming area started from early October to November, coinciding with the occurrence of anomalous NSCC[7] (Fig. 7). Kelp juvenile sporophytes were more vulnerable to variable external environments, including high light, compared to larger size class sporophytes[39]. The lower SSC allowed solar radiation to penetrate the upper water column, contributing to better light conditions. Strong ultraviolet radiation could damage proteins and lead to radical oxygen formation of kelp juvenile sporophytes[40,41]. On the other hand, the chl-a concentration displayed its highest value in November 2021 (Fig. 8e), indicating the influence of red tide blooms (Fig. 7). After the red tide blooms, the nutrients along the coast of the Shandong Peninsula were depleted, resulting in a relative oligotrophic condition (Fig. 3). The phosphorus limitation conditions were confirmed after anomalous kelp mortality events[10]. Laboratory cultivation also demonstrated that the growth rate of kelps from the farming area would increase with the addition of nutrients[10]. Thus, the oligotrophic condition caused by red tide blooms might play an important role in kelp mortality events. Typically, in a stratified water column, the decomposition of organic matter following phytoplankton blooms tends to consume dissolved oxygen and result in hypoxia conditions at the bottom layer. This condition is not favorable for the growth of other plankton species. However, the shallow water depth in the Rongcheng offshore area, combined with wind-mixing, prevents the development of hypoxia environments (Supplementary Fig. S7a, d). Therefore, dissolved oxygen is not the primary factor contributing to kelp mortality. Additionally, sudden reductions in salinity have been shown to damage local macroalgae species in nearshore areas[42]. In the autumn of 2021, an extreme rainfall event occurred in coastal eastern Australia, diluting salinity and leading to the death of kelp sporophytes[43]. Flood-induced reduction in salinity was considered the primary cause of the mass mortality of kelp sporophytes[43]. While a direct correlation between Yellow River discharge and unit yield was not established (Fig. 8f), it remained viable to transport fresher water to the aquaculture area via NSCC. The anomalous low salinity may also play an important role in the kelp mortality event (Supplementary Fig. S7c). Therefore, the lower salinity, stronger light conditions, and insufficient nutrients (especially phosphorus limitation conditions) are the direct cause of the extremely serious kelp mortality offshore of the eastern Shandong Peninsula. The anomalous intrusion of NSCC and the migration of red tide blooms with NSCC, driven by the extreme rainfall event in the inland of North China in the autumn of 2021, were accountable for the changes in marine environmental factors and the occurrence of kelp mortality events mentioned above.

Summary and implications

Natural climate variability changes (e.g., extreme weather events) accelerated the frequency of the impact of human activities on the natural ecological ecosystem. During the past decades, chemical fertilizer application in the Huang-Huai-Hai agricultural area led to an increase in soil nutrient stocks[21]. As a result, excessive nutrient discharges were closely associated with the frequent occurrence of phytoplankton blooms in the Bohai Sea[44]. The extreme rainfall events broke the nutrient trade-off between land agriculture (inland area) and marine (coastal area) aquaculture, accelerating the migration of terrestrial nutrient materials and resulting in coastal

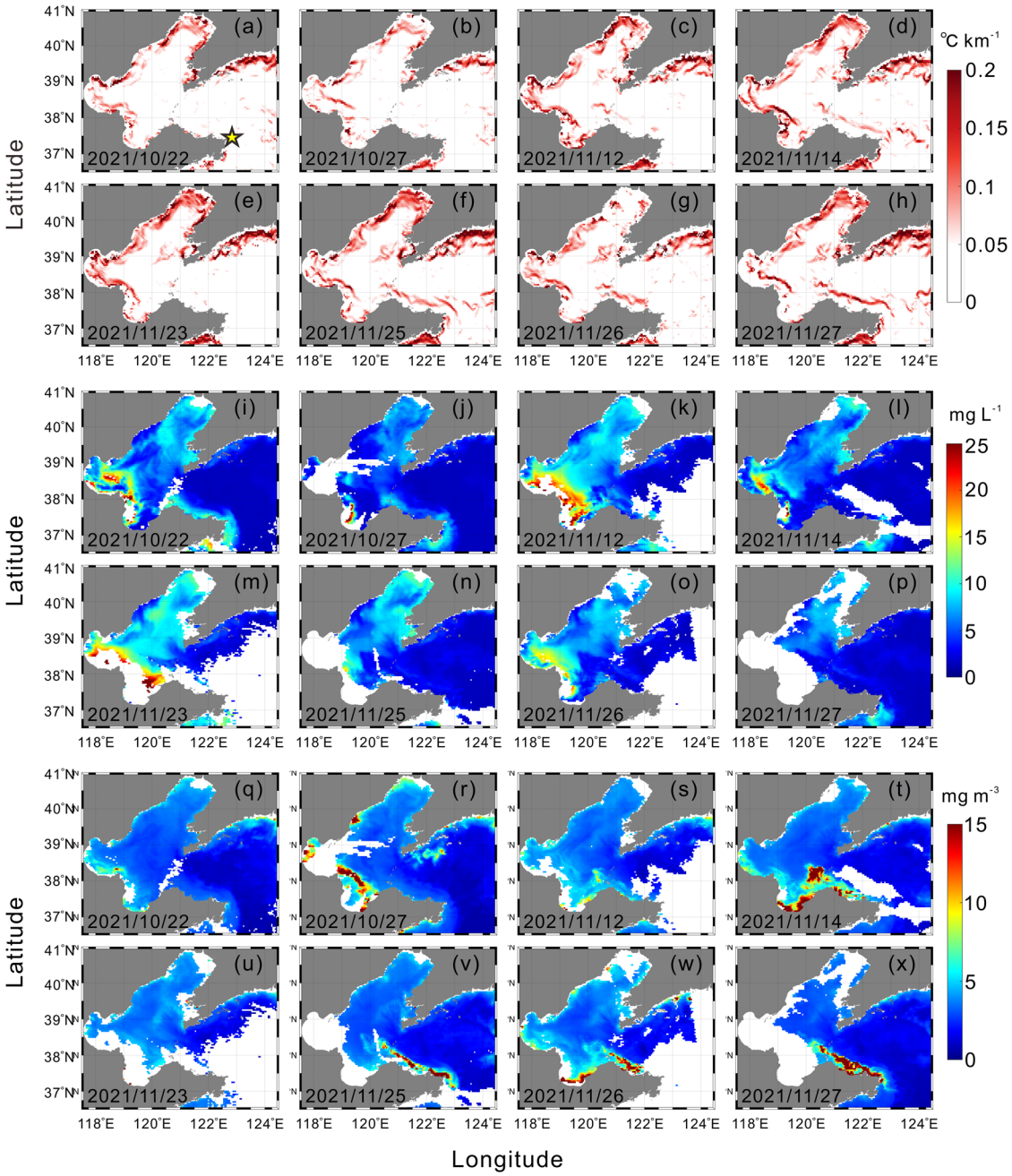

Fig. 7 | Time series of MODIS-derived sea surface parameters over the Bohai and North Yellow Sea in autumn 2021. a–h MODIS derived available daily SSTG (°C km^{-1}), **i–p** MODIS derived available daily SSC (mg L^{-1}), and **q–x** MODIS derived available daily chl-a concentration (mg m^{-3}). The yellow star in **a** indicates the Cape Chengshan (Northeast end of Shandong Peninsula). The white areas are masked by clouds or bad results from the retrieve algorithm.

ecological deterioration. Here, joint multidisciplinary observations provided a successive and full picture of the cascading effects within marine ecosystems (Fig. 9). An extreme autumn rainfall event in remote North China caused an unexpected flood in the Yellow River watershed, leading to increased riverine transport of nutrients and resulting in an exceptionally high DIN/DIP ratio (indicative of phosphorus limitation) in the Bohai Sea. Meanwhile, the NSCC was diluted and characterized by anomalous low turbidity. The phosphorus limitation condition of the NSCC was alleviated when it extended to the North Yellow Sea along the coast of Shandong Peninsula, as it encountered the DIP-rich coastal water. This led to the occurrence and expansion of red tide blooms at the frontal zone of the coastal currents. The red tide blooms in the frontal zone, consuming a large amount of nutrients. At the same time, NSCC drove this frontal zone to gradually migrate eastward along the north coast of the Shandong Peninsula, continuously removing nutrients from the coastal seawater, resulting in a sharp decrease in nutrient content in the coastal seawater that the frontal zone passed through. Then, the lower salinity, stronger light conditions caused by NSCC, and the nutritional competition caused by red tide blooms led to unexpected devastating kelp mortality events offshore of the eastern Shandong Peninsula.

Different from the regular summer flood patterns, extreme rainfall derived pulsed floods and anomalous NSCC in the autumn season of 2021. By coincidence, the vulnerable kelp seedlings were transferred from workshops to kelp farming areas during this season. The deterioration of the marine environment precipitated a substantial mortality rate among kelp juveniles, which in turn led to an almost extinction of kelp yield in the subsequent year. It seemed like the ingenious cooperation of various conditions resulted in such huge kelp mortality. Nonetheless, it was precisely the

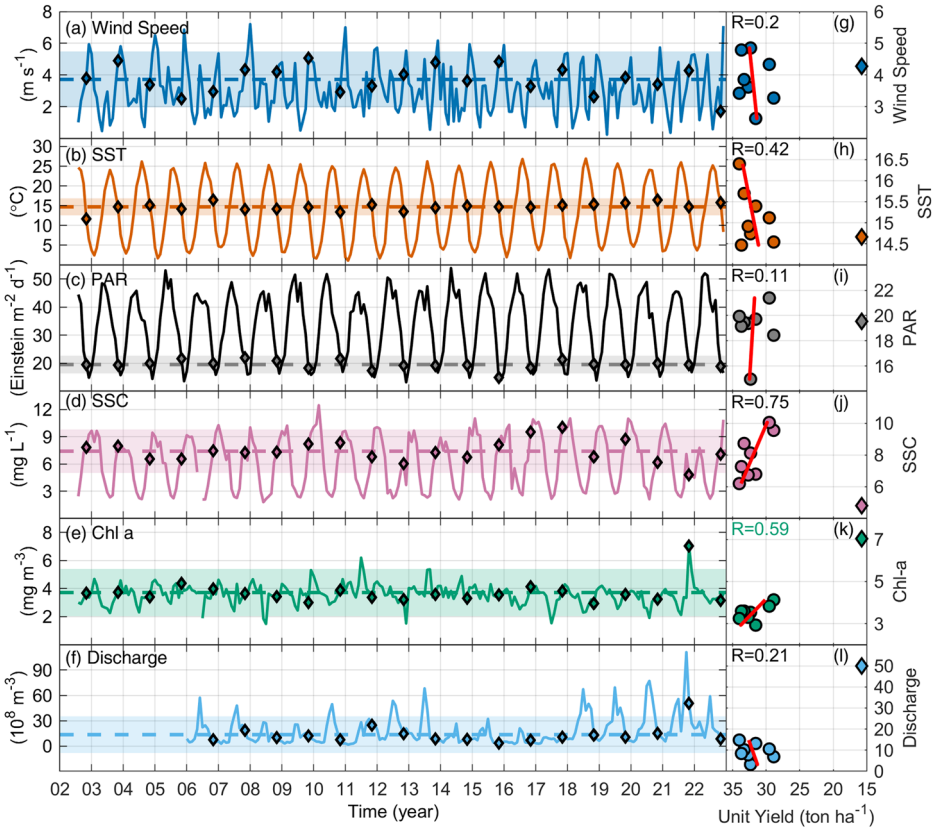

Fig. 8 | Monthly variation of hydrological characteristics and their relationship with unit yield of kelp. a–f Monthly variation of wind speed (**a**), SST (**b**), PAR (**c**), SSC (**d**), chl-a concentration averaged over the Rongcheng offshore area (36.8–37.5°N, 122–123°E) and discharge of the Yellow River (**f**) in the last 21 years (2002–2022). The solid diamonds in **a**–**f** indicate the corresponding parameters in November. The dashed lines indicate the climatic averaged values of November, and the colorful bands indicate the range of mean value plus or minus 2 standard deviations of the corresponding parameters. **g**–**l** Lag-correlation between the hydrological characteristics and unit yield of kelp in next year for 2014–2021. The red solid lines depict the regression fitting. The solid diamonds in **g**–**l** indicate corresponding parameters in November of 2021.

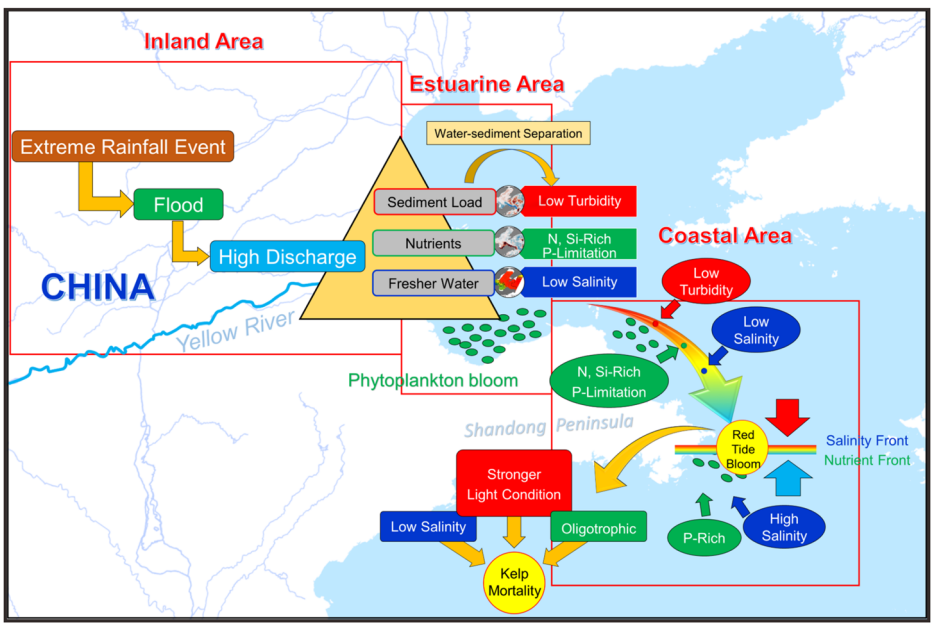

Fig. 9 | Mechanism of teleconnection of extreme rainfall events in North China to coastal ecological disasters. An extreme rainfall event that occurs inland results in flooding and soared river discharge, large quantities of sediments, nutrients and freshwater being transported to the Bohai and North Yellow Sea. The water-sediment separation accounts for the low turbidity of estuarine fresher water. The optimal nutrient conditions contribute to the red tide bloom along the salinity fronts and nutrient fronts formed between the coastal currents (DIN, DSi-rich) and the offshore saline water (DIP-rich). The transportation of coastal currents leads to the migration of the optimal nutrient conditions and red tide blooms along the coast of the Shandong Peninsula. The lower salinity, stronger ultraviolet radiation caused by limpid coastal current, and relative oligotrophic conditions caused by red tide bloom contributed to extremely serious kelp disasters on the eastern Shandong Peninsula.

unpredictability of extreme weather events that was prone to such unexpected ecological degradation. Observing, analyzing, and projecting such events present considerable challenges to human beings' adaptation strategies against climate change due to the uncertainty of their timing and location, relatively short observation records, and data deficiencies. This reminds us of the necessity and urgency of comprehensive observations from multiple disciplines and methods to reveal the Earth system's response to unexpected extreme weather events. Cascading effects within the marine ecosystem from extreme weather events should be fully considered in future projections.

More importantly, this autumn extreme rainfall event was ascribed to the combined effects of SSTAs in the tropical Indo-Pacific-Atlantic Ocean[17,45]. The warm SSTAs in the Indo-Pacific warm pool and equatorial central-eastern Pacific contribute to or intensify the westward extension of WNPSH and anomalous autumn rainfall, while the warm SSTAs in the tropical Atlantic anchor the position of extreme rainfall event in North China. It revealed the teleconnection of low-latitude tropical SSTAs to mid-latitude coastal ecosystems through extreme rainfall events under climate change[46]. As the frequency and severity of extreme weather events increased under global warming, more and more unexpected marine environmental

problems would arise in the future. Enhanced comprehension of cascading feedback within ecosystems instigated by extreme events was critical for addressing these unanticipated alterations. Therefore, a truly Integrated Earth Observation System from multidisciplinary cooperation was more needed to monitor unexpected changes and enhance human risk management capabilities for increasing extreme weather events.

Materials and methods

Field sampling and laboratory analysis

Cruise surveys were conducted across the Bohai and North Yellow Sea (55 stations) during the autumn season (October 27, 2021–November 04, 2021) onboard the R/V Chuangxin I (Fig. 1). At each station, the SBE-911plus CTD system (Sea-Bird Electronics Inc., U.S.) was deployed to obtain vertical hydrographic profiles of temperature, salinity, chlorophyll-a fluorescence (chl-a; WET Labs ECO-AFL/FL fluorometer sensor), and turbidity (WET Labs ECO-NTU turbidity sensor). Four typical sections were selected to present the vertical distribution of water column characteristics (Supplementary Fig. S1). Section A was distributed along the Bohai Bay and Laizhou Bay, while section B denoted the Bohai Strait. Section C represented the Chengshantou-Dalian line, and section D crossed the central North Yellow Sea.

Discrete water samples were collected from surface (0–3 m), middle (half of water depth), and bottom (1–3 m above the seabed) layers using Niskin sampling bottles attached to the CTD system. The water samples (1 L) were filtered through 47 mm Whatman GF/F filters for chl-a analysis. The filters were frozen at -20 °C in the dark and subsequently extracted in 90% acetone. Laboratory analysis of chl-a was conducted using a TD-700 fluorometer (Turner Designs)[47,48]. There was a good consistency between the chl-a fluorescence measured in situ by the CTD sensors (chl-a-S) and chl-a concentration measured in the lab (chl-a-L) (R = 0.80; Supplementary Fig. S8). Then we calibrated the chl-a-S with chl-a-L based on their linear relationship. For nutrient measurement, water samples (1 L) at each layer were filtered onboard through Whatman 0.45 μm cellulose acetate membranes. Nutrient concentrations, including DIN, DIP, and DSi, were analyzed in the laboratory using flow injection analysis (AA3, Bran + Luebbe, Germany). The DIN is the sum of NO_2^-, NO_3^- and NH_4^+. DIP and DSi are the concentration of total inorganic dissolved phosphorus (PO_4-P) and silicate ($Si(OH)_4$). The limits of detection were 0.015 μM L^{-1} for NO_3^-, 0.003 μM L^{-1} for NO_2^-, 0.04 μM L^{-1} for NH_4^+, 0.02 μM L^{-1} for DIP, and 0.03 μM L^{-1} for DSi[49].

Furthermore, a surface buoy observation system at station YS16 was deployed Rongcheng offshore area to monitor environmental fluctuations induced by the intrusion of NSCC (Supplementary Fig. S1). The hydrodynamic parameters (including temperature, salinity, and dissolved oxygen) in surface layer (1 m depth) were recorded by ACTW-CAR or AROW2-CAR sensors (JFE Advantech) at buoy station YS16. The wind speed at 3 m above the sea surface, was recorded by the Young wind monitor MA-05106 (RM Young). Unfortunately, the dissolved oxygen concentration for 2020 was not accessible due to a sensor malfunction. All these data were obtained from the Yellow Sea ocean observation and research station of the Chinese Academy of Sciences, with a temporal resolution of 1 hour.

Data processing

In addition to the observations at discrete stations, the RDI 300 kHz ADCP transducer was mounted on the research vessel (3 m below the water surface in the measurements) in a downward-looking configuration, continuously recording current velocity and acoustic backscatter data in bottom-tracking mode. The 10-minute averaged ADCP data were the average of 165 continuous pings with a temporal interval of 4 s, using a bin size of 1 m, with the first layer located 4.12 m away from the transducer. A slant angle of 20° produced a strong echo, contaminating the signal across the seafloor layer. Accordingly, 6% of the near-bottom data were excluded from further analyses. Additionally, ADCP data with a correlation below 128 counts and PG4 (percent good) values less than 75% were excluded from the analysis to ensure data quality.

The tidal currents and amplitudes in the study area were obtained by TPXO tide models established by Oregon State University[50]. The model included eight major harmonic constituents (M2, S2, N2, K2, K1, O1, P1, Q1) on a 1/30° resolution grid. MATLAB package Tide Model Driver was utilized to extract tidal currents. Tidal amplitudes at gauge stations Yantai and Weihai were compared with tidal heights provided by the Tide Tables 2021 (Supplementary Fig. S9), edited by the National Marine Data and Information Service[51]. The quality and credibility of the two datasets were confirmed by their good consistency. Field observations and model results indicated that the tidal currents in the study area were dominated by barotropic tidal currents, with the energy of baroclinic tidal currents accounting for only 5% on the northern coast of the Shandong Peninsula[52]. To eliminate the influence of tidal currents, the residual current was derived by subtracting Tide Model Driver derived total barotropic tidal velocities from the original shipboard ADCP measurements based on time and coordinate. The water-mass volume backscattering strength (S_v; dB) recorded by the ADCP was used to represent the SSC[53,54]. On 2 November 2021, the current velocity and S_v recorded by the ADCP were presented to check the hydrodynamic characteristics of the NSCC along the northern coast of the Shandong Peninsula (Fig. 6).

Open-access data

Open-access reanalysis datasets were employed to identify the long-term trends of sea surface properties and monitor red tide blooms over the study area (Supplementary Table S1). The monthly average wind data were derived from the NCEP/NCAR Reanalysis 1 dataset (https://www.esrl.noaa.gov/psd/data/gridded/data.ncep.reanalysis.html) provided by the NOAA/OAR/ESRL PSD, Boulder, Colorado, USA. High- resolution LANDSAT-8 images were downloaded from the US Geological Survey (USGS) database through the Global Visualization Viewer (http://glovis.usgs.gov/) to track variations in water properties.

The daily and monthly average SST, Remote Sensing Reflectance at 555 nm (Rrs555), PAR, and chl-a products (2002–2022) were derived from the NASA MODIS level 3 products (https://oceancolor.gsfc.nasa.gov). The Level 3 products featured a spatial resolution of 4.63 km. Then, the position and strength of the temperature fronts were determined[55]:

$$SSTG = \sqrt{\left(\frac{\partial T}{\partial x}\right)^2 + \left(\frac{\partial T}{\partial y}\right)^2} \quad (1)$$

SSTG represented sea surface temperature gradient (°C km^{-1}). T represents the *SST*, and *x* and *y* indicate the direction of east and north, respectively. The Rrs555 was usually used as a substitute index of water turbidity because their exponential relationship[56–58]. Here, we converted the Rrs555 to SSC based on the result of Liu et al.[58] (SSC = Exp (101.8 × Rrs555) × 1.301). In addition, the chl-a concentration was used to track traces of red tides since there was a strong relationship between them[59]. Satellite-derived chl-a concentrations were generally overestimated in turbid coastal waters, due to the influence of dissolved organic matter on remote sensing reflectance[60,61]. However, it was found the overestimation had an upper limit value (10 mg m^{-3}) in Chinese coastal seas[57], which could be used as a threshold to identify phytoplankton blooms to avoid false blooms caused by turbid waters. Here, we took it as the standard for identifying phytoplankton blooms.

Statistical data from official releases helped us to clarify regional climate change and hydrological variability characteristics. The aquaculture area and yield of kelp in Shandong province were mainly from the China Fisheries Statistical Yearbook. The yearly rainfall data were derived from China Water Resources Bulletin and China Climate Bulletin. The river discharge and sediment flux recorded at gauging stations of Lijin and Haihezha were supplied by the Yellow River Conservancy Commission (http://www.yrcc.gov.cn/) and the Bulletin of Chinese River Sediment compiled by the Ministry of Water Resources of the People's Republic of China. In addition, the monthly concentration of riverine TDN and TDP for

2021 at gauging stations of Lijin were obtained from the China National Environmental Monitoring Centre (http://www.cnemc.cn/en/). The TDN and TDP were measured by the alkaline potassium sulfate method[62]. The monthly nutrient fluxes of 2021 were obtained by multiplying the concentrations of TDN and TDP by the river discharge. Although the riverine nitrogen-to-phosphorus ratio (TDN/TDP) was different from the nitrogen-to-phosphorus ratio from the cruise survey (DIN/DIP), it still reflected the impact of extreme rainfall events on the nutrient status of rivers. The distribution and time of duration of red tide blooms during 2021 were supplied by the Bulletin of China Marine Disaster (2021) compiled by the Ministry of Natural Resources of the People's Republic of China. Economic loss statistics resulted from extreme rainfall events were derived from Ministry of Emergency Management of the People's Republic of China. The distribution of agricultural regions and river basins were derived from Resource and Environment Science and Data Center at the Institute of Geographical Sciences and Natural Resources Research, Chinese Academy of Sciences (https://www.resdc.cn). The population data of each province was from the National Bureau of Statistics according to the Seventh National Population Census (http://www.stats.gov.cn).

In this study, the climate mean state of each parameter was computed by averaging the multi-year data (2002–2022). The anomalies indicated the difference between the individual values and the climate mean state values. In addition, the juvenile kelp was generally transformed from the hatchery to the sea during the autumn season, and subsequently harvested in the spring through to the summer of the subsequent year[63]. Considering that the rapid increase in kelp unit yield after 2014 may be related to the innovation of farming technology, we conducted a lag-correlation analysis between hydrological environmental parameters (including wind speed, SST, PAR, SSC, chl-a and Yellow River discharge) and unit yield of kelp from 2014 to 2021, i.e., the relationship between environmental parameters in November each year and unit yield of kelp in the next year (Fig. 8g–l).

Data availability

The data that support the findings of this study are available in figshare Repository (https://doi.org/10.6084/m9.figshare.24418267)[64].

Received: 22 October 2023; Accepted: 24 April 2024;
Published online: 07 May 2024

References

1. Crossland, C. J., Kremer, H. H., Lindeboom, H., Crossland, J. I. M. & Tissier, M. D. A. Coastal fluxes in the Anthropocene: the land-ocean interactions in the coastal zone project of the International Geosphere-Biosphere Programme. (Springer Berlin, Heidelberg, 2005).
2. Weissenberger, S. & Chouinard, O. The vulnerability of coastal zones towards climate change and sea level rise. *In:* Adaptation to climate change and sea level rise (pp. 7–31). (Springer, Dordrecht, 2015).
3. Masson-Delmotte, V. et al. Climate change 2021: the physical science basis. Contribution of working group I to the sixth assessment report of the intergovernmental panel on climate change, 2 (2021).
4. Thompson, V. et al. The 2021 western North America heat wave among the most extreme events ever recorded globally. *Sci. Adv.* **8**, eabm6860 (2022).
5. Chen, C. T. A. et al. Enhanced buoyancy and hence upwelling of subsurface Kuroshio waters after a typhoon in the southern East China Sea. *J. Mar. Syst.* **42**, 65–79 (2003).
6. Teagle, H., Hawkins, S. J., Moore, P. J. & Smale, D. A. The role of kelp species as biogenic habitat formers in coastal marine ecosystems. *J. Exp. Mar. Biol. Ecol.* **492**, 81–98 (2017).
7. Zhang, J. Seaweed industry in China. Obtenido de Innovation Norway China: https://www.submariner-network.eu/images/grass/Seaweed_Industry_in_China.pdf (2018).
8. Li, D., Gao, Z., Song, D., Shang, W. & Jiang, X. Characteristics and influence of green tide drift and dissipation in Shandong Rongcheng coastal water based on remote sensing. *Estuar. Coast. Shelf Sci.* **227**, 106335 (2019).
9. State Oceanic Administration of the People's Republic of China. Bulletin of China marine disasters in 2021 (in Chinese). (2022).
10. Li, X. et al. Comprehensive analyses of large-scale saccharina japonica damage in the principal farming area of Rongcheng Shandong Province in 2021-2022. *J. Agric. Sci. Technol.* **25**, 206–222 (2023).
11. Zhao, G., Jiang, W., Wang, T., Chen, S. & Bian, C. Decadal variation and regulation mechanisms of the suspended sediment concentration in the Bohai Sea, China. *J. Geophys. Res. Oceans.* **127**, e2021JC017699 (2022).
12. Guo, J., Pan, H., Cao, R., Wang, J., & Lv, X. Multiple timescale variations in water transparency in the eastern China seas over the period 1997–2019. *J. Geophys. Res. Oceans*. **128**, e2022JC019170 (2023).
13. Zhou, Y. et al. Variations of water transparency and impact factors in the Bohai and Yellow Seas from satellite observations. *Remote Sens.* **13**, 514 (2021).
14. He, C. et al. Enhanced or weakened western North Pacific subtropical high under global warming? *Sci. Rep.* **5**, 16771 (2015).
15. Zhou, T. J. & Yu, R. C. Atmospheric water vapor transport associated with typical anomalous summer rainfall patterns in China. *J. Geophys. Res. Atmos.* **110**, D08104 (2005).
16. Kosaka, Y., Chowdary, J. S., Xie, S. P., Min, Y. M. & Lee, J. Y. Limitations of seasonal predictability for summer climate over East Asia and the Northwestern Pacific. *J. Climate.* **25**, 7574–7589 (2012).
17. Liu, B., Zhu, C., Ma, S. & Yan, Y. Combined effects of tropical Indo-Pacific-Atlantic SST anomalies on record-breaking floods over Central-North China in September 2021. *J. Clim.* **35**, 6191–6205 (2022).
18. Wang, Q. et al. Evaluations of submarine groundwater discharge and associated heavy metal fluxes in Bohai Bay. *China. Sci. Total Environ.* **695**, 133873 (2019).
19. Wang, X., Li, H., Zhang, Y., Zheng, C. & Gao, M. Investigation of submarine groundwater discharge and associated nutrient inputs into Laizhou Bay (China) using radium quartet. *Mar. Pollut. Bull.* **157**, 111359 (2020).
20. Liu, S. Response of nutrient transports to water-sediment regulation events in the Huanghe basin and its impact on the biogeochemistry of the Bohai. *J. Mar. Syst.* **141**, 59–70 (2015).
21. Tao, Y., Wei, M., Ongley, E., Li, Z. & Jingsheng, C. Long-term variations and causal factors in nitrogen and phosphorus transport in the Yellow River, China. *Estuar. Coast. Shelf Sci.* **86**, 345–351 (2010).
22. Wu, N., Liu, S. M., Zhang, G. L. & Zhang, H. M. Anthropogenic impacts on nutrient variability in the lower Yellow River. *Sci. Total Environ.* **755**, 142488 (2021).
23. Yang, F., Wei, Q., Chen, H. & Yao, Q. Long-term variations and influence factors of nutrients in the western North Yellow Sea, China. *Mar. Pollut. Bull.* **135**, 1026–1034 (2018).
24. Wang, J., Yu, Z., Wei, Q. & Yao, Q. Long-term nutrient variations in the Bohai Sea over the past 40 years. *J. Geophys. Res. Oceans.* **124**, 703–722 (2019).
25. Zheng, L. W., Zhai, W. D., Wang, L. F. & Huang, T. Improving the understanding of central Bohai Sea eutrophication based on wintertime dissolved inorganic nutrient budgets: Roles of north Yellow Sea water intrusion and atmospheric nitrogen deposition. *Environ. Pollut.* **267**, 115626 (2020).
26. Li, X., Chen, H., Jiang, X., Yu, Z. & Yao, Q. Impacts of human activities on nutrient transport in the Yellow River: the role of the water-sediment regulation scheme. *Sci. Total Environ.* **592**, 161–170 (2017).
27. Redfield, A. C. The biological control of chemical factors in the environment. *Am. Sci.* **46**, 230A–221 (1958).
28. Yang, Z. & Liu, J. A unique Yellow River-derived distal subaqueous delta in the Yellow Sea. *Mar. Geol.* **240**, 169–176 (2007).

29. Lin, X. et al. An asymmetric upwind flow, Yellow Sea warm current: 1. New observations in the western Yellow Sea. *J. Geophys. Res.-Oceans*. **116**, C04026 (2011).
30. Liu, L. & Wang, Z. Temporal and spatial distributions and formation mechanism of suspended sediment in the coastal area of the Shandong Peninsula. *Mar. Sci.* **43**, 55–65 (2019).
31. Zheng, X. et al. The features and mechanisms of the North Shandong Coastal Current: a case study in 2014. *J. Oceanogr.* **77**, 631–646 (2021).
32. Lü, T. et al. The coastal front modulates the timing and magnitude of spring phytoplankton bloom in the Yellow Sea. *Water Res.* **220**, 118669 (2022).
33. Ding, X. et al. Unprecedented phytoplankton blooms in autumn/winter in the southern Bohai Sea (China) due to high Yellow River discharge: Implications of extreme rainfall events. *J. Environ. Manage.* **351**, 119901 (2024).
34. Bollen, M., Pilditch, C. A., Battershill, C. N. & Bischof, K. Salinity and temperature tolerance of the invasive alga Undaria pinnatifida and native New Zealand kelps: Implications for competition. *Mar. Biol.* **163**, 1–14 (2016).
35. Mabin, C. J., Johnson, C. R. & Wright, J. T. Physiological response to temperature, light, and nitrates in the giant kelp Macrocystis pyrifera from Tasmania. *Australia. Mar. Ecol. Prog. Ser.* **614**, 1–19 (2019).
36. Tom Dieck, I. Temperature tolerance and survival in darkness of kelp gametophytes (Laminariales, Phaeophyta) ecological and biogeographical implications. *Mar. Ecol. Prog. Ser.* **100**, 253–264 (1993).
37. Dring, M. J., Wagner, A. & Luening, K. Contribution of the UV component of natural sunlight to photoinhibition of photosynthesis in six species of subtidal brown and red seaweeds. *Plant Cell Environ.* **24**, 1153–1164 (2001).
38. Kerrison, P. D., Stanley, M. S., Edwards, M. D., Black, K. D. & Hughes, A. D. The cultivation of European kelp for bioenergy: site and species selection. *Biomass Bioenerg.* **80**, 229–242 (2015).
39. Gao, X., Endo, H., Nagaki, M. & Agatsuma, Y. Interactive effects of nutrient availability and temperature on growth and survival of different size classes of Saccharina japonica (Laminariales, Phaeophyceae). *Phycologia* **56**, 253–260 (2017).
40. Dring, M. J., Makarov, V., Schoschina, E., Lorenz, M. & Lüning, K. Influence of ultraviolet-radiation on chlorophyll fluorescence and growth in different life-history stages of three species of Laminaria (Phaeophyta). *Mar. Biol.* **126**, 183–191 (1996).
41. Müller, R., Desel, C., Steinhoff, F. S., Wiencke, C. & Bischof, K. UV-radiation and elevated temperatures induce formation of reactive oxygen species in gametophytes of cold-temperate/Arctic kelps (Laminariales, Phaeophyceae). *Phycol. Res.* **60**, 27–36 (2012).
42. Peteiro, C. & Sánchez, N. Comparing salinity tolerance in early stages of the sporophytes of a non-indigenous kelp (Undaria pinnatifida) and a native kelp (Saccharina latissima). *Russ. J. Mar. Biol.* **38**, 197–200 (2012).
43. Davis, T. R. et al. Extreme flooding and reduced salinity causes mass mortality of nearshore kelp forests. *Estuar. Coast. Shelf Sci.* **275**, 107960 (2022).
44. Zheng, L. W. & Zhai, W. D. Excess nitrogen in the Bohai and Yellow seas, China: distribution, trends, and source apportionment. *Sci. Total Environ.* **794**, 148702 (2021).
45. Yang, K. et al. Increased variability of the western Pacific subtropical high under greenhouse warming. *Proc. Natl. Acad. Sci.* **119**, e2120335119 (2022).
46. Na, Y. & Lu, R. The concurrent record-breaking rainfall over Northwest India and North China in September 2021. *Adv. Atmos. Sci.* **40**, 653–662 (2023).
47. Lorenzen, C. J. Determination of chlorophyll and pheo-pigments: spectrophotometric equations. *Limnol. Oceanogr.* **12**, 343–346 (1967).
48. Lin, L. et al. Effect of wind on summer chlorophyll-a variability in the Yellow Sea. *Front. Mar. Sci.* **9**, 1104258 (2023).
49. Liu, X. et al. Temporal and spatial variations and impact factors of nutrients in Bohai Bay, China. *Mar. Pollut. Bull.* **140**, 549–562 (2019).
50. Egbert, G. D. & Erofeeva, S. Y. Efficient inverse modeling of barotropic ocean tides. *J. Atmos. Ocean. Technol.* **19**, 183–204 (2002).
51. NMDS (National Marine Data and Information Service). Tidal Tables 2021, Vol. 1 From the Yalu River Mouth to the Changjiang River Mouth. China Ocean Press, Beijing. (2020).
52. Yu, H., Bao, X., Zhu, X., Chen, X. & Wu, D. Analysis of the high-resolution observed current data in the southern area of the North Huanghai Sea in summer. *Acta Oceanol. Sin.* **30**, 12–20 (2008).
53. Deines, K. L. Backscatter estimation using broadband acoustic Doppler current profilers. *In:* Proceedings of the IEEE sixth working conference on current measurement (Cat. No. 99CH36331) pp. 249–253 (1999).
54. Wall, G. R., Nystrom, E. A. & Litten, S. Use of an ADCP to compute suspended-sediment discharge in the tidal Hudson River, New York (No. 2006-5055) (2006).
55. Belkin, I. M. & O'Reilly, J. E. An algorithm for oceanic front detection in chlorophyll and SST satellite imagery. *J. Mar. Syst.* **78**, 319–326 (2009).
56. Yuan, D., Zhu, J., Li, C. & Hu, D. Cross-shelf circulation in the Yellow and East China Seas indicated by MODIS satellite observations. *J. Mar. Syst.* **70**, 134–149 (2008).
57. He, X. et al. Satellite views of the seasonal and interannual variability of phytoplankton blooms in the eastern China seas over the past 14 yr (1998–2011). *Biogeosciences* **10**, 4721–4739 (2013).
58. Liu, X., Qiao, L., Zhong, Y., Xue, W. & Liu, P. Multi-year winter variations in suspended sediment flux through the Bohai Strait. *Remote Sens.* **12**, 4066 (2020).
59. Hao, Y. J., Tang, D. L., Yu, L. & Xing, Q. G. Nutrient and chlorophyll a anomaly in red-tide periods of 2003–2008 in Sishili Bay, China. *Chin. J. Oceanol. Limnol.* **29**, 664–673 (2011).
60. O'Reilly, J. E. et al. Ocean color chlorophyll algorithms for SeaWiFS. *J. Geophys. Res.: Oceans* **103**, 24937–24953 (1998).
61. Dierssen, H. M. Perspectives on empirical approaches for ocean color remote sensing of chlorophyll in a changing climate. *Proc. Natl. Acad. Sci.* **107**, 17073–17078 (2010).
62. Wang, Y. et al. Impact of water-sediment regulation scheme on seasonal and spatial variations of biogeochemical factors in the Yellow River estuary. *Estuar. Coast. Shelf Sci.* **198**, 92–105 (2017).
63. Li, J., Bergman, K., Thomas, J. B. E., Gao, Y. & Gröndahl, F. Life cycle assessment of a large commercial kelp farm in Shandong. *China. Sci. Total Environ.* **903**, 166861 (2023).
64. Li, W., Wang, Z., Cui, Q., Sun, X., & Huang, H. Influence of extreme rainfall event in North China on coastal ecosystem data sets. *figshare* https://doi.org/10.6084/m9.figshare.24418267 (2023).

Acknowledgements

This work was supported by the Chinese Academy of Sciences (XDB42010203), the National Natural Science Foundation of China (42176090, 42306059), the Key Laboratory of Marine Geology and Environment, Chinese Academy of Sciences (MGE2021KG07), the China Postdoctoral Science Foundation (2020M682246) and the Postdoctoral Applied Research Project of Qingdao. Data acquisition and sample collection were carried out onboard the R/V Chuangxin I of the Yantai Institute of Coastal Zone Research, Chinese Academy of Sciences. The buoy observation data were Supported by the Yellow Sea ocean observation and research station of the Chinese Academy of Sciences. The authors would also like to thank the captain, crew members, and scientists aboard the R/V Chuangxin I for their cooperation and help.

Author contributions

W.L. contributed to conceptualization, formal analysis, and writing (original draft). Z.W. contributed to conceptualization, data curation, formal analysis, supervision, and writing (review & editing). Q.C, X.S. contributed to data curation and investigation, and writing (review & editing). H.H. contributed to supervision.

Competing interests

The authors declare no competing interests.

Additional information

Supplementary information The online version contains supplementary material available at https://doi.org/10.1038/s43247-024-01418-3.

Correspondence and requests for materials should be addressed to Zhenyan Wang.

Peer review information *Communications Earth & Environment* thanks Anette Engesmo and the other, anonymous, reviewer(s) for their contribution to the peer review of this work. Primary Handling Editors: Carolina Ortiz Guerrero. A peer review file is available.